Incorporating Vegetation Under the Collector Roof of a Solar Chimney Power Plant

Johannes P. Pretorius[a] and Detlev G. Kröger[b]
Received 17 April 2007 and accepted 22 January 2008

The incorporation of vegetation under the collector roof of a large-scale solar chimney power plant is investigated as a potential secondary (agricultural) plant function. The effect on plant performance when incorporating vegetation over two radial collector distances is evaluated. Additionally, the influence on plant performance when modelling the air (with certain vapour content) inside the chimney and atmosphere surrounding the plant according to different temperature lapse rates is considered. Results predict that the incorporation of vegetation in the solar chimney power plant is potentially possible, but its inclusion will cause major reductions in plant power output.

Nomenclature

Roman

A	Area (m^2)
b	Exponent
C	Coefficient
c	Specific heat capacity (J/kgK)
d	Diameter (m)
e	Emissivity
g	Gravitational acceleration (9.8 m/s^2)
H	Height (m)
h	Convective heat transfer coefficient (W/m^2K)
I	Solar irradiation (W/m^2)
i	Latent heat of vaporization (J/kg)
K	Loss coefficient
k	Thermal conductivity (W/mK)
m	Mass-flow rate (kg/s)
n	Refractive index or number
P	Pitch (m)
Pr	Prandtl number
p	Pressure (N/m^2)
q	Heat flux (W/m^2)
R	Gas constant (J/kgK)
r	Radius (m) or resistance (s/m)
T	Temperature (K or °C)
t	Thickness (m)
v	Velocity (m/s)
z	Height above ground level or depth in ground (m)

Greek symbols

α	Absorptivity
γ	Psychrometric constant
γ^*	Adjusted psychrometric constant
Δ	Slope of saturated vapour pressure line (N/m^2K)
ε	Roughness (m)
η	Efficiency (%)
μ	Dynamic viscosity (kg/ms)
ξ	Temperature gradient (K/m)
ρ	Density (kg/m^3)
τ	Transmittance
φ	Relative humidity (%)
ω	Absolute humidity (kg H_2O / kg dry air)

Subscripts

a	Ambient air
avg	Average
b	Beam
bw	Bracing wheel
c	Chimney
$cond$	Conduction
d	Diffuse
e	Extinction or effective
fg	Fluid to gas
g	Ground
gh	Ground surface to collector air
H	Heat transfer
h	Horizontal surface
i	Inlet
m	Mean or mixture
net	Net
p	Constant pressure
r	Roof or radial
s	Support or stomata or saturated
sat	Saturated
sc	Saturation commences
sD	Support drag
T	Temperature
t	Tangential
tg	Turbo-generator
$turb,i$	Turbine inlet
V	Vapour transfer
v	Water vapour
ve	Vegetation
veh	Vegetation to air under collector roof
ver	Vegetation to collector roof
w	Water
wb	Wet-bulb

[a] jp.pretorius@eskom.co.za, Eskom, PO Box 1091, 2000 Johannesburg

[b] Department of Mechanical Engineering, University of Stellenbosch, Private Bag X1, 7602 Matieland

1. Introduction

A solar chimney power plant consists of a transparent circular canopy or roof located at a certain height above the ground, with a chimney or circular tower at its centre (figure 1). The chimney houses one or more turbines at its base, (each) connected to an electric generator. Solar radiation penetrates the collector roof and heats the ground surface beneath, which in turn heats the adjacent air. The warm air under the roof flows towards and up into the chimney. The air flowing through the chimney drives the turbo-generator(s), which subsequently generates electricity.

2. Literature Review

Haaf et al.[1] discuss the basic principles behind the operation,

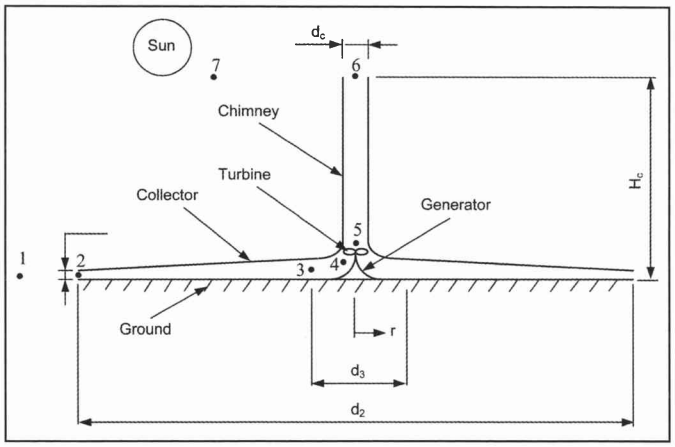

Figure 1: Schematic illustration of a solar chimney power plant

construction and power generation of a solar chimney power plant, while Haaf[2] presents preliminary test results from a prototype plant built in Manzanares, Spain in 1982. Schlaich[3] endorses the use of solar chimney power plants for future electricity generation and also communicates details of the construction, materials, operation, tests and experimental data of the pilot solar chimney plant in Manzanares. Pasumarthi and Sherif[4] published an approximate mathematical model for a solar chimney, followed by a subsequent article (Pasumarthi and Sherif[5]) which validates the model against experimental results from the pilot plant. Kröger and Buys[6] and Gannon and Von Backström[7] perform early comprehensive analyses on the performance of solar chimney power plants, while Gannon and Von Backström[8] also conduct a study concerning solar chimney turbine performance. An analytical and numerical model is developed by Bernardes et al.[9], presenting a comparison between simulated results and experimental measurements from the pilot plant at Manzanares. Bernardes et al.[9] also conduct a sensitivity analysis on, among other things, the influence of varying the collector roof transmissivity and heat penetration coefficient on plant performance. Pastohr et al.[10] conduct a basic temperature and flow field analysis using a numerical CFD package and compare their results to another simple numerical model. A relatively detailed numerical model is developed by Pretorius et al.[11], simulating the performance of a large-scale reference solar chimney power plant. A mathematical model is also developed by Bilgen and Rheault[12] for evaluating the performance of solar chimney power plants at high latitudes. A refined numerical model for simulating large solar chimney plants is presented by Pretorius and Kröger[13], while Pretorius and Kröger[14] also conduct a sensitivity analysis on the operating and technical specifications of a solar chimney power plant.

The current study employs the numerical model and specified reference plant (see Appendix of this paper) as presented by Pretorius and Kröger[13].

3. Approach

The question of whether a large-scale solar chimney power plant is financially viable solely as a power generating facility remains unanswered. The idea of adding value to the solar chimney system through the pursuit of secondary ventures has in recent times come to the fore. One such venture involves the solar collector taking on a secondary function as a greenhouse for agricultural purposes. If this is found to be viable, farmers could grow their crops in certain areas under the collector roof.

This paper investigates the possibility of including vegetation under the collector roof of the solar chimney power plant. Equations are derived for determining the rate of evapotranspiration from the vegetation surface. Simulations are then performed, evaluating the effect on plant performance when incorporating vegetation. In addition, the influence on plant performance is evaluated when modelling the air (with certain vapour content) inside the chimney and atmosphere surrounding the plant according to different temperature lapse rates.

Relevant conservation equations for the introduction of vegetation into the existing numerical model (from Pretorius and Kröger[13]) are based on the governing equations derived by Pretorius and Kröger[13].

4. Modification under Collector Roof

With the inclusion of vegetation in the collector of the solar chimney power plant, the existing numerical model (from Pretorius and Kröger[13]) must be modified. As is evident from figure 2, the collector is effectively divided into two sections, namely the vegetation and ground section. It is assumed that the vegetation will be planted around the entire circumference (360°) of the collector, inwards from the collector perimeter to a specified radius, r_{ve}. Planting vegetation nearer to the perimeter of the collector allows vegetation to be included under the collector roof, while eliminating the possibility that the vegetation may be scorched by the high collector temperatures near the chimney.

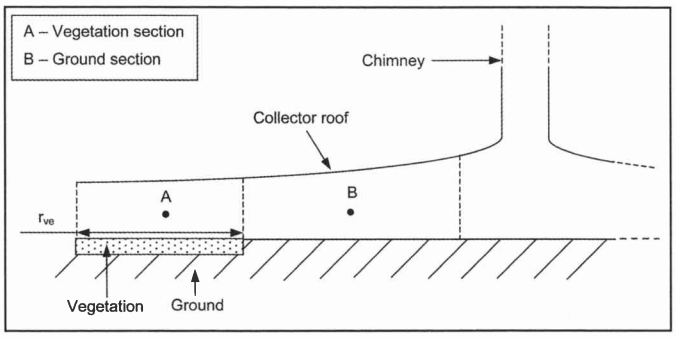

Figure 2: Definition of sections created in the collector by the inclusion of vegetation

5. Determining the Rate of Evapotranspiration

As the air under the collector roof flows over and through the vegetation, it will absorb moisture from the plants and the accompanying ground surface (in which they grow). In order to evaluate the effect of vegetation on the performance of a solar chimney power plant, it is necessary to determine the rate at which the water vapour is absorbed. This rate is known as the rate of evapotranspiration. Note that all thermophysical properties are evaluated for an air-vapour mixture, from the relations by Kröger[15].

According to Monteith and Unsworth[16], the rate of evapotranspiration can be evaluated using

$$\left(\frac{m_v}{A}\right) i_{fg} = \frac{\Delta_{avg} I_{net} + (vpd) h_{veh}}{\Delta_{avg} + \gamma^*} \quad (1)$$

known as the Penman-Monteith equation, where (m_v/A) is the rate of water evaporation from the transpiring surface per unit area, i_{fg} is the latent heat of evaporation, Δ_{avg} is the average slope of the saturated vapour pressure line, I_{net} is the net radiation absorbed by the vegetation, vpd is the vapour pressure depression,

also known as vapour pressure deficit, h_{veh} is the convective heat transfer coefficient from the transpiring surface to the collector air and γ^* is the adjusted psychrometric constant.

The latent heat of evaporation on the left-hand-side of Eq. (1) is determined at the vegetation surface temperature. By assuming the collector air and water vapour to be ideal gases, the Clapeyron-Clausius equation can be used to find the average slope of the saturated vapour pressure line, as follows (Çengel and Boles[17])

$$\Delta_{avg} \approx \left(\frac{dp}{dT}\right)_{sat} = \frac{i_{fg}\, p_{sat}}{T_{avg}^2 R_v} \tag{2}$$

where R_v is the gas constant for water vapour. The terms i_{fg} and p_{sat} of Eq. (2) represent the latent heat of evaporation and the saturated vapour pressure respectively and both are evaluated at the average between the dry-bulb and wet-bulb air temperatures:

$$T_{avg} = \frac{1}{2}(T + T_{wb}) \tag{3}$$

The saturated vapour pressure is calculated from an equation by Kröger[15], as follows

$$p_{sat} = 10^z \tag{4}$$

where

$$\begin{aligned} z = {} & 10.79586\left(1 - 273.16/T_{avg}\right) + 5.02808 \log_{10} \\ & \left(273.16/T_{avg}\right) + 1.50474 \times 10^{-4} \\ & \left[1 - 10^{-8.29692\left(\left(T_{avg}/273.16\right) - 1\right)}\right] \\ & + 4.2873 \times 10^{-4}\left[10^{4.76955\left(1 - \left(273.16/T_{avg}\right)\right)} - 1\right] \\ & + 2.786118312 \end{aligned} \tag{5}$$

The net radiation absorbed by the vegetation is calculated as follows:

$$I_{net} = \left(\tau_e \alpha_{ve}\right)_b I_{hb} + \left(\tau_e \alpha_{ve}\right)_d I_{hd} - q_{ver} - q_{cond} \tag{6}$$

where τ_e is the effective transmittance of the glass collector roof, α_{ve} is the absorptivity of the vegetation surface under the collector roof, I_h is the solar radiation on a horizontal surface, q_{ver} is the radiation exchange of the vegetation with the collector roof and q_{cond} is the energy conducted into or out of the ground. The subscripts b and d denote the beam and diffuse solar radiative components respectively while the brackets in Eq. (6) represent the transmittance-absorptance product of the vegetation.

The vapour pressure depression (deficit) is defined as the difference between the actual vapour pressure and the saturation pressure at the same dry-bulb air temperature and is given by

$$vpd = p_{sat} - p_v \tag{7}$$

The saturated vapour pressure (p_{sat}) of Eq. (7) is determined from Eq. (4) and (5) at the dry-bulb collector air temperature. According to Çengel and Boles[17], the actual vapour pressure is ascertained by

$$p_v = \phi\, p_{sat} \tag{8}$$

where φ is the relative humidity of the collector air. Çengel and Boles[17] also present the following relation for evaluating the relative humidity

$$\phi = \frac{\omega\, p}{\left(0.622 + \omega\right) p_{sat}} \tag{9}$$

where p is the total air pressure under the collector roof and ω is the absolute air humidity, which is determined from a derived water vapour continuity equation (not presented here).

The convective heat transfer coefficient h_{veh} is evaluated analogously to a strategy discussed in the paper by Pretorius and Kröger[13] for evaluating h_{gh} (the convective heat transfer coefficient from the ground surface to the air under the collector roof of the solar chimney power plant). The above-mentioned publication presents two heat transfer relations for determining the convective heat transfer coefficient from large horizontal surfaces. These equations were developed by Kröger and Burger[18] and Burger[19] for a smooth flat surface and employ respective skin friction coefficients of $c_f = 0.0052$ and $c_f = 0.0044$. However, according to Westdyk[20], by substituting an equivalent friction coefficient of 0.023971 for these skin friction values, h_{veh} can be more accurately calculated for air-flow over a particular vegetation surface (short grass). This equivalent friction coefficient is also employed in the calculation of the vegetation surface shear stress term. When implementing these changes, one finds the following alternative forms of the equations by Burger[19]:

$$h_{veh} = \frac{\left[0.2106 + 0.011986 v\left(\frac{\rho T_m}{\mu g\, \Delta T}\right)^{1/3}\right]}{\left[\frac{\mu T_m}{g\, \Delta T\, c_p\, k^2 \rho^2}\right]^{1/3}} \tag{10}$$

$$h_{veh} = 3.87 + 0.011986\left(\frac{v \rho c_p}{\mathrm{Pr}^{2/3}}\right) \tag{11}$$

where T_m is the mean of the vegetation surface and dry-bulb collector air temperature, while ΔT is the difference between these two temperatures. All properties of Eq. (10) and (11) are evaluated for an air-vapour mixture at the mean temperature. It should be noted that these two equations do not necessarily represent the physics of evapotranspiration, but do however satisfy the Penman-Monteith equation and also compare well with the heat transfer coefficient values found by other researchers.

Conradie[21] gives the following relation for the determination of the psychrometric constant:

$$\gamma = \frac{c_{p,ma}\, p}{0.622\, i_{fg,wb}} \tag{12}$$

where $c_{p,ma}$ is the specific heat capacity of the air-vapour mixture (evaluated at the dry-bulb collector air temperature) and $i_{fg,wb}$ is the latent heat of evaporation evaluated at the wet-bulb collector air temperature.

According to Monteith and Unsworth[16], the resistance to vapour transfer experienced by plant leaves are the sum of a boundary layer resistance r_V and a stomatal resistance r_s. The boundary layer resistance depends on the leaf dimensions and wind speed over them, while the stomatal resistance depends on the geometry, size and spacing of stomatal pores on the leaves. Monteith and Unsworth[16] consider r_V equal to the resistance to heat transfer (r_H) of the leaf, giving the following equation for the adjusted psychrometric constant

$$\gamma^* = \left(\frac{r_V + r_s}{r_H}\right)\gamma = \left(1 + \frac{r_s}{r_H}\right)\gamma \tag{13}$$

The resistance to heat transfer of the leaves is determined by

$$r_H = \frac{\rho c_{p,ma}}{h_{veh}} \tag{14}$$

where ρ is the density of the air-vapour mixture. Both the density and specific heat of Eq. (14) are evaluated at the mean of the vegetation surface and dry-bulb air temperatures. According to the Food and Agriculture Organization of the United Nations (FAO)[21], the value of r_s for a reference grass crop is 70 s/m. The numerical model assumes a similar value for the stomatal surface resistance of the vegetation under the collector roof.

6. Temperature Lapse Rates for Moist Air

The reference plant of this paper (see Appendix) assumes a dry adiabatic lapse rate (DALR) for the air inside the chimney and the atmosphere surrounding the solar chimney power plant. These are believed to be good approximations of the experienced temperature gradients in these regions when dry atmospheric air is assumed. Kröger[15] presents the following relations, describing the temperature and pressure distributions for dry air with respect to height as predicted by the DALR

$$T = T_1 - \frac{dT}{dz} z = T_1 - 0.00975 z \tag{15}$$

$$p = p_1 \left[1 - 0.00975 \left(\frac{z}{T_1} \right) \right]^{3.5} \tag{16}$$

where T and p represent the respective air temperature and pressure at a specific height z above ground level, with T_1 and p_1 the temperature and pressure at ground level.

When vegetation is included under the collector roof, the air flowing through the solar chimney power plant will absorb moisture from the vegetation surface. Therefore, the assumption of a DALR inside the chimney becomes invalid. According to Kröger[15], the respective atmospheric temperature and pressure distributions for air containing water vapour are

$$T = T_1 - \frac{0.00975(1+\omega)z}{(1+1.9\omega)} \tag{17}$$

$$p = p_1 \left[1 - \frac{0.00975(1+\omega)z}{(1+1.9\omega)T_1} \right]^{2.1778(1+1.9\omega)/(\omega+0.622)} \tag{18}$$

where ω is the absolute humidity of the air.

When moist air is raised in a gravitational field, the air cools down adiabatically until it reaches the saturation point. If the air should rise even further, cooling will cause the vapour in the air to condense and precipitate. The energy removed from the condensate then heats the surrounding air. Kröger[15] gives the following temperature and pressure distribution relations for moist air that experiences condensation at a certain height above ground level

$$T_s = T_{sc} + \xi_T z_s \tag{19}$$

$$p_s = p_{sc} \left(1 + \frac{\xi_T z_s}{T_{sc}} \right)^{-0.021233(1+\omega_{sc})/[\xi_T(\omega_{sc}+0.622)]} \tag{20}$$

where T_s and p_s represent the temperature and pressure at a specific height z_s, which is the height above the elevation where condensation commences. The terms T_{sc}, p_{sc} and ω_{sc} refer to the respective temperature, pressure and absolute humidity of the air at the point above ground level where condensation commences. The symbol ξ_T is the air temperature gradient after condensation commences and is given by

$$\xi_T = \frac{dT_s}{dz} = \frac{-\dfrac{(1+\omega_s)g}{\left\{ \dfrac{0.42216\times10^{-11}\omega_s p_s \exp(5406.1915/T_s) i_e}{[(\omega_s+0.622)RT_s]} \right\}}}{c_{p,ma} + 3.6693\times10^{-8}\omega_s p_s \exp(5406.1915/T_s)/T_s^2} \tag{21}$$

where T_s, p_s and ω_s indicate the respective temperature, pressure and absolute humidity of the air after condensation has occurred. The term $c_{p,ma}$ refers to the specific heat capacity of the air-vapour mixture and is determined by

$$c_{p,ma} = c_{pa} + \omega_s c_{pv} \tag{22}$$

where c_{pa} and c_{pv} are the specific heats of dry air and saturated water vapour respectively. Furthermore, i_e of Eq. (21) is determined from

$$i_e = i_{fgw0} - (c_{pw} - c_{pv})(T_s - 273.15) \tag{23}$$

where i_{fgw0} is the latent heat of water at 273.15 K and c_{pw} is the specific heat capacity of saturated water liquid. All specific heats of Eq. (22) and (23) are determined at T_s /2.

Note that Eq. (21) cannot be analytically integrated. However, Kröger[15] states that this temperature gradient, determined at a particular pressure and temperature, hardly changes at higher elevations where both the pressure and temperature will be lower, i.e. the temperature gradient is approximately constant.

7. Plant Specifications

The solar chimney power plant model of this section is based on the reference plant specifications listed in the Appendix. In addition, vegetation is included under the collector roof over part of the ground surface area (see figure 2), with dimensions as specified in table 1.

Vegetation	
Density	ρ_{ve} = 1900 kg/m^3
Specific heat capacity	c_{ve} = 2200 J/kgK
Thermal conductivity	k_{ve} = 2 W/mK
Emissivity	e_{ve} = 0.98
Absorptivity	α_{ve} = 0.77
Surface roughness	ε_{ve} = 0.1 m
Depth	z_{ve} = 0.55 m
Radial distance from perimeter	r_{ve} = 1978 m or 1012 m

Table 1: Average properties of wet soil according to Mills[23], emissivity of relatively short grass (0.1 m to 0.15 m) according to Dong et al.[24] and absorptivity of grass (80 % to 90 % new, green grass) according to Hsu[25]

The numerical model assumes the following vegetation properties. The vegetation density, specific heat and thermal conductivity are assumed to be similar to those of wet soil and are presented in table 1, as given by Mills[23]. The vegetation

emissivity and absorptivity are assumed to be similar to the properties of relatively short grass and are included in the same table, as given respectively by Dong et al.[24] and Hsu[25].

8. Assumptions

The simulations of this section are based on the following assumptions:

- ❑ The vegetation in the collector is approximated as wet soil.
- ❑ It is assumed that the depth of the vegetation reaches approximately 0.5 m deep into the ground. Therefore, properties are assumed to be that of vegetation from the surface to 0.5 m and that of dry ground deeper than 0.5 m (for the vegetation section of the collector as illustrated by figure 2).
- ❑ The vegetation is assumed to be constantly wet (by irrigation), thereby approximating the water vapour mass-flow to the collector air as a source term.
- ❑ No water is transferred from the vegetation to the collector air during night-time.
- ❑ If condensation occurs in the collector, the addition of water to the vegetation or ground through condensation is assumed to be negligible.
- ❑ The maximum temperature at which vegetation can function without impairing the photosynthetic processes is assumed to be 40°C (assumed somewhat lower to values found by Taiz and Zeiger[26]).
- ❑ Unless stated otherwise, the numerical model employs an atmosphere outside the solar chimney power plant that considers the effect of water vapour in the air. Therefore, Eq. (17) and (18) are implemented for the air outside the plant. It is assumed that no condensation takes place in the atmosphere surrounding the plant.
- ❑ Unless stated otherwise, the numerical model considers the effects of water vapour and possible condensation for the air inside the chimney of the solar chimney power plant. Therefore, Eq. (17) and (18), together with Eq. (19) and (20) (should condensation occur) are implemented for the air inside the chimney of the plant.

9. Simulation and Results

Two computer simulations are performed, employing the above-mentioned plant specifications, vegetation properties and assumptions. This section investigates the incorporation of vegetation under the collector roof from the collector perimeter to respective radii of r_{ve} = 1978 m and r_{ve} = 1012 m.

Including vegetation over approximately 2000 m of the collector radius

From figure 3 it is clear that the inclusion of vegetation in the collector over a radial distance of 1978 m has a major effect on the power output of the solar chimney power plant. This is confirmed by table 2, which shows a reduction of 45.1 % in annual power output for the plant incorporating vegetation, compared to the reference plant.

As air flows under the collector roof from the perimeter to the chimney, water from the vegetation surface is evaporated. The evaporation process cools the vegetation surface as well as the collector air. With lower collector air temperatures, a lower plant driving potential results, ultimately causing a lower power output compared to the reference plant.

Plant configuration	Annual power output [GWh]
Reference plant	336
Plant with vegetation	184.4

Table 2: Annual power output comparison, illustrating the effect of incorporating vegetation under the collector roof, over a radial distance of 1978 m from the collector perimeter

Figure 3 also presents less smooth power output curves for the plant incorporating vegetation compared to the curves for the reference plant. As mentioned, the inclusion of vegetation lowers the collector air temperatures and driving potential. This makes the plant susceptible to variations in ambient conditions, which cause the illustrated small fluctuations in power output. Note that both plant models (reference plant model and model incorporating vegetation) are subject to the same ambient conditions. However due to the fact that the reference plant operates at much higher driving potentials (as a result of higher collector air temperatures), the reference plant is less sensitive to changes in the ambient conditions.

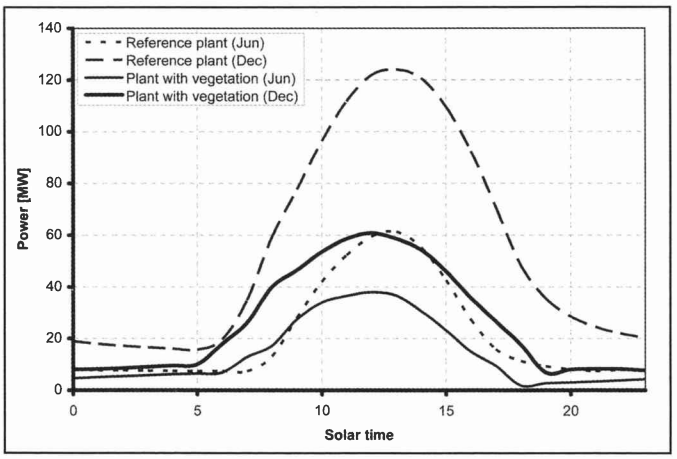

Figure 3: Daily solar chimney power output profile, illustrating the influence of including vegetation under the collector roof, over a radial distance of 1978 m from the collector perimeter

Two other factors which contribute to the uneven output profiles are the heat transfer due to evaporation from the vegetation surface and the fact that the plant model incorporating vegetation implements temperature lapse rates which consider the variable humidity of the air inside and outside the plant.

Figure 4 illustrates, on a psychrometric chart, how the air flowing under the collector roof is heated and humidified in the vegetation section and simply heated in the ground section of the collector (see Figure 2). The curves indicate the conditions

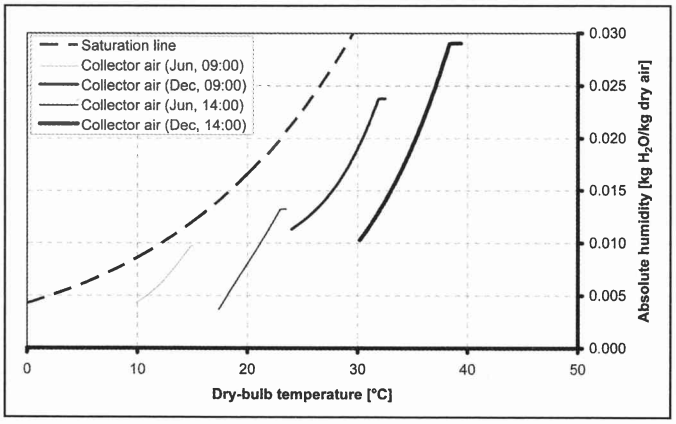

Figure 4: The psychrometric chart, illustrating the heating and humidification and simple heating of the collector air at 09:00 and 14:00 on 21 June and 21 December, for r_{ve} = 1978 m

in the collector at 09:00 and 14:00 on a typical day in June and December. As a large part of the collector employs vegetation (r_{ve} = 1978 m), heating and humidification takes place over a substantial radius from the collector perimeter. Simple heating of the collector air takes place over a small section of the collector (where a ground surface is employed) and is indicated by the small horizontal sections at the tips of the curves in Figure 4.

The curves of figure 5 represent the vegetation or ground surface temperature and relative humidity of the collector air throughout the collector at 09:00 on 21 June and 21 December. The temperature curves indicate a slight rise in vegetation surface temperature from the perimeter of the vegetation section (also perimeter of collector, at r = 2500 m) to the end of the vegetation section (r = 522 m). Thereafter, a jump in temperature results, indicating the start of the ground section. A minor increase in temperature is evident from this point on to the end of the ground section (r = 200 m). It is clear that the average ground surface temperature is significantly higher than the average vegetation surface temperature.

Figure 5 also shows that the relative humidity of the collector air increases steadily over the vegetation section, as water from the vegetation surface is evaporated and absorbed by the flowing air. In the ground section, higher air temperatures are experienced due to higher (ground) surface temperatures and no water vapour is added to the collector air in this section. This causes a subsequent steady decrease in the relative humidity of the air over the ground section.

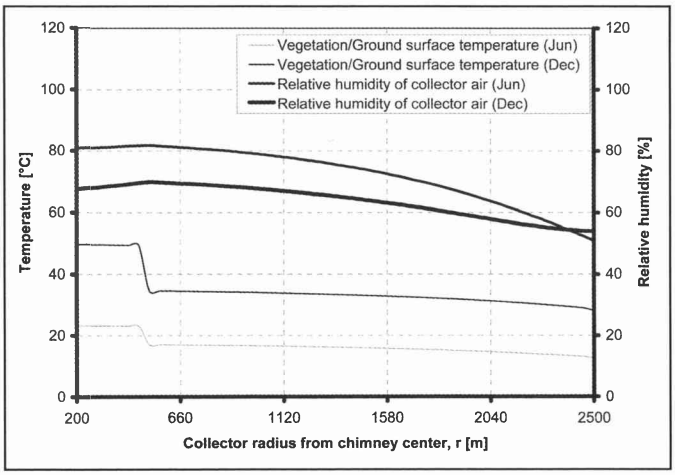

Figure 5: Vegetation or ground surface temperature and relative humidity of the collector air throughout the collector at 09:00 on 21 June and 21 December , for r_{ve} = 1978 m

In addition, the average relative humidity of the collector air is somewhat higher during winter than the average humidity during summer. During winter the collector air is cooler than during summer and consequently cannot hold as much moisture as the warmer collector air during summer, which explains the higher relative humidity values during winter.

The curves of figure 6 represent the vegetation or ground surface temperature and relative humidity of the collector air throughout the collector at 14:00 on 21 June and 21 December. Trends, similar to those in figure 5, are observed. Furthermore, surface temperatures are notably higher and relative humidities are somewhat lower at 14:00, compared to their corresponding values at 09:00 (from figure 5).

It is very important to observe from figure 6 that the vegetation surface temperature reaches 40°C (at 14:00 in December) at a collector radius of approximately r = 1300 m and rises even further to the end of the vegetation section. As mentioned in the previous section, a rise in vegetation temperature above 40°C is assumed to adversely affect the photosynthetic and other processes of the plants. This suggests that, for the given location, vegetation should not be incorporated to a collector radius beyond r = 1300 m from the collector perimeter.

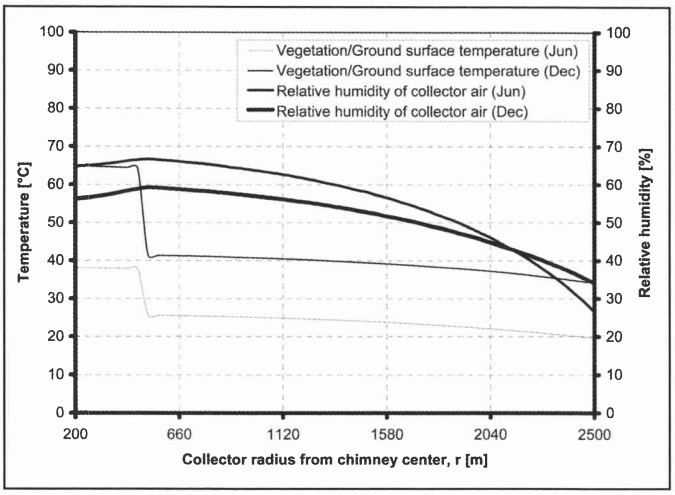

Figure 6: Vegetation or ground surface temperature and relative humidity of the collector air throughout the collector at 14:00 on 21 June and 21 December, for r_{ve} = 1978 m

Including vegetation over approximately 1000 m of the collector radius

Though significantly reduced compared to the results of figure 3 and table 2, figure 7 indicates that the inclusion of vegetation in the collector over a radial distance of 1012 m still has a major adverse effect on the power output of the solar chimney power plant. Table 3 confirms this, showing a reduction of 29.8% in annual power output for the plant incorporating vegetation, compared to the reference plant.

Plant configuration	Annual power output [GWh]
Reference plant	336
Plant with vegetation	236

Table 3: Annual power output comparison, illustrating the effect of incorporating vegetation under the collector roof, over a radial distance of 1012 m from the collector perimeter

The performance curves of figure 7 are also smoother than the curves presented in figure 6, for the plant models incorporating vegetation. With a greater section of the collector employing a ground surface, higher air temperatures are experienced in the collector, giving an increased plant driving potential. This makes the plant less sensitive to fluctuations in ambient temperatures and causes smoother power output profiles.

Figure 8 presents similar trends to those in figure 4. However, as vegetation is only included over a radial distance of r_{ve} = 1012 m from the collector perimeter, heating and humidification take place over a smaller section of the collector, while simple heating in the ground section is significantly more prominent (represented by the horizontal sections of the curves).

Figures 9 and 10 also present similar trends to those of figures 5 and 6. It is however clear that vegetation is employed over a smaller collector section. The temperature curves of figure 9 and 10 indicate a slight rise in vegetation surface temperature

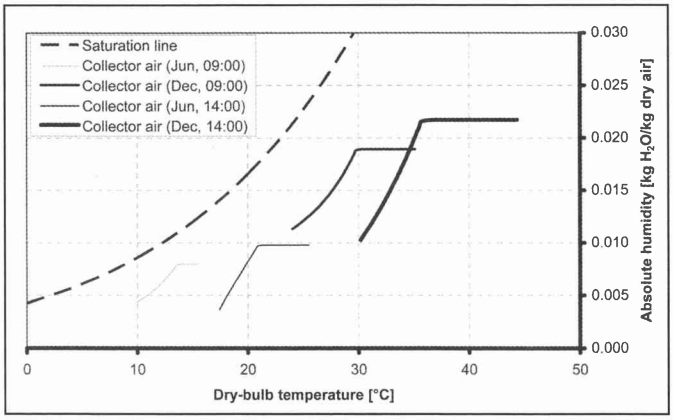

Figure 8: The psychrometric chart, illustrating the heating and humidification and simple heating of the collector air at 09:00 and 14:00 on 21 June and 21 December, for r_{ve} = 1012 m

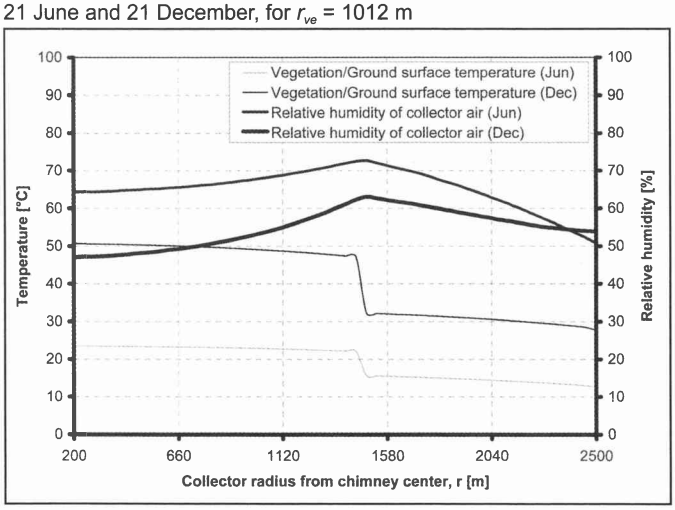

Figure 9: Vegetation or ground surface temperature and relative humidity of the collector air throughout the collector at 09:00 on 21 June and 21 December, for r_{ve} = 1012 m

from the perimeter of the vegetation section (also perimeter of collector, at r = 2500 m) to the end of the vegetation section (r=1488 m). Thereafter, a jump in temperature results, indicating the start of the ground section. A steady increase in temperature is evident from this point on to the end of the ground section (r = 200 m). Correspondingly, the relative humidity of the collector air increases steadily over the vegetation section and decreases over the ground section.

Note from figure 10 that when incorporating vegetation to a collector radius of only r_{ve} = 1012 m, the vegetation surface temperature always remains below 40°C.

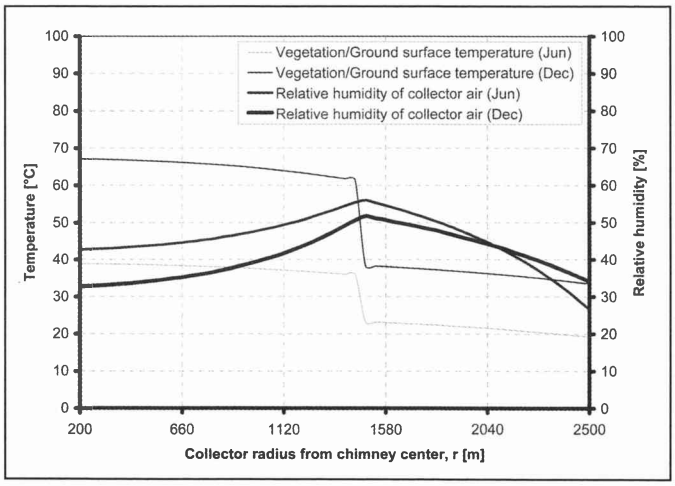

Figure 10: Vegetation or ground surface temperature and relative humidity of the collector air throughout the collector at 14:00 on 21 June and 21 December, for r_{ve} = 1012 m

10. Temperature Lapse Rate Effects

This section evaluates the influence of employing various temperature lapse rates for the atmosphere outside and the air inside the chimney of the solar chimney power plant. As mentioned in the previous section on temperature lapse rates for moist air, the reference solar chimney power plant of this paper employs a dry adiabatic lapse rate (DALR) for the atmosphere outside and air inside the chimney of the plant. However, when incorporating vegetation under the collector roof of the plant, the effects of water vapour in air have to be taken into account, a factor which the DALR does not consider. This necessitates the inclusion of temperature lapse rates which do consider the effects of water vapour. Two such lapse rates are discussed in the section on temperature lapse rates for moist air.

A publication by Kröger and Blaine[27] also investigated the effects of water vapour and possible condensation in a large solar chimney power plant (using the same equations of this paper's section on temperature lapse rates for moist air). The authors conclude that moist air improves plant driving potential and that condensation may occur inside the chimney of the plant under certain conditions.

11. Simulation and Results

Numerical simulations are performed for three plant models, all employing the previously mentioned plant specifications, vegetation properties and assumptions (except for the last two assumptions, which are varied here) of this paper. The first model employs a DALR for the outside atmosphere and the air inside the chimney (according to Eq. (15) and (16)). The second model takes the effect of water vapour in air into account, for the ambient air as well as for the air inside the chimney of the plant (according to Eq. (17) and (18)). The third plant model also takes into account the effect of water vapour in the air inside and outside the plant, while additionally considering the possible condensation of the air inside the chimney of the plant (according to Eq. (17), (18), (19) and (20)). Simulations are performed for a plant including vegetation over radial distances of r_{ve} = 1978 m and r_{ve} = 1012 m from the collector perimeter.

The results of the first plant model are referred to as "DALR",

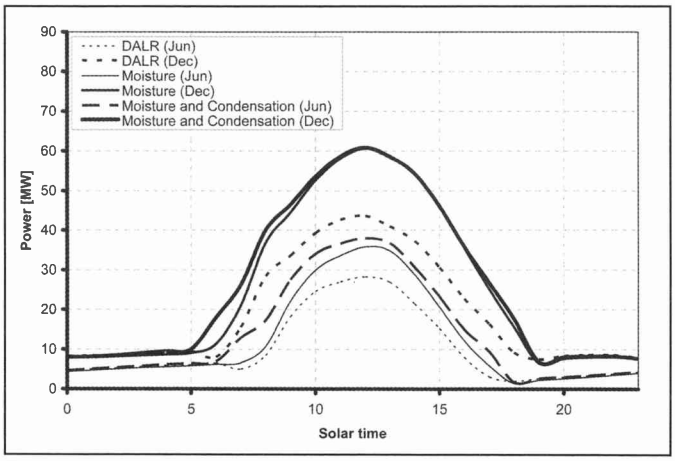

Figure 11: Daily solar chimney power output for a plant employing vegetation under the collector roof over a radial distance of r_{ve} = 1978 m; effect of different temperature lapse rate models on plant performance

those of the second model as "Moisture" and those of the third as "Moisture and Condensation". It should be noted that all of the above-mentioned models employ vegetation under the collector roof of the plant and consider the transfer of water vapour from the vegetation to the collector air. Thus, their only distinction lie in the way which the respective temperature (and corresponding pressure) lapse rates are modelled.

From figure 11 it is clear that all the plant models predict similar power outputs during night-time, while the models considering the effects of water vapour predict significantly higher plant power production during the day. During the night, the lapse rates which consider water vapour employ the same absolute humidity for the air outside and inside the chimney of the plant. Consequently, during night-time driving potentials are predicted which are similar to the driving potentials of the plant model employing a DALR. During the day however, the air flowing under the collector roof absorbs moisture from the vegetation, thereby significantly altering the vapour content of the air inside the chimney of the plant (while the humidity of the outside air is assumed constant). The increased vapour content of the air inside the chimney alters the pressure distribution of the chimney air, causing an increased plant driving potential and ultimately power output. This corresponds to the findings of Kröger and Blaine[27].

Plant configuration	Annual power output [GWh]
DALR	131.8
Moisture	168.6
Moisture and Condensation	184.4

Table 4: Annual power output comparison for a plant incorporating vegetation under the collector roof over a radial distance of 1978 m; effect of different temperature lapse rate models on plant performance

Another noticeable trend from figure 11 is the increased power output of the "Moisture and Condensation" plant model during early mornings in summer and for most of the day during winter. During these times, condensation occurs inside the chimney of the plant. Again, this corresponds to the findings of Kröger and Blaine[27]. When the water vapour in the chimney air condenses, heat is transferred to the air, thereby altering the chimney air temperature and corresponding pressure distribution. This causes an increased plant driving potential and ultimately power output. The annual power output in table 4 confirms these results.

Figure 12 and table 5 present results for a plant incorporating vegetation over a smaller radial distance (1012 m). Similar trends, though much reduced, are visible compared to figure 11 and table 4. With less vegetation implemented under the collector of the plant, less moisture is transferred to the collector air via evapotranspiration. This results in a smaller difference in vapour content between the air outside and inside the chimney of the plant. Consequently, a smaller difference in driving potential and subsequent power output is predicted for the "Moisture" and "Moisture and Condensation" models, compared to the "DALR" model.

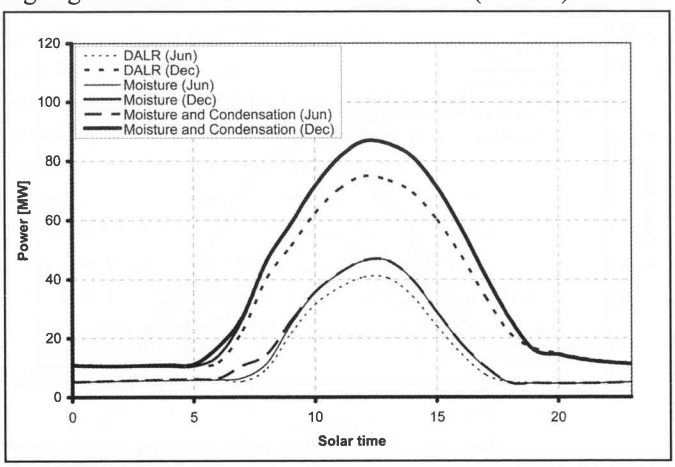

Figure 12: Daily solar chimney power output for a plant employing vegetation under the collector roof over a radial distance of r_{ve} = 1012 m; effect of different temperature lapse rate models on plant performance

Plant configuration	Annual power output [GWh]
DALR	205
Moisture	232.5
Moisture and Condensation	236

Table 5: Annual power output comparison for a plant incorporating vegetation under the collector roof over a radial distance of 1012 m; effect of different temperature lapse rate models on plant performance

12. Conclusion

The incorporation of vegetation under the collector roof of a solar chimney power plant is investigated for possible agricultural purposes. Vegetation is initially included over a collector radius of approximately 2000 m and results predict that the maximum allowable vegetation surface temperature of 40°C is exceeded over this distance. Furthermore, a major reduction in annual power output of approximately 45 % is shown when incorporating vegetation under the collector roof over such a large collector radius. Vegetation is then included in the model over a collector radius of approximately 1000 m. In this particular case, results indicate that vegetation surface temperatures never exceed 40°C, while a major reduction in annual yield of approximately 30 % is still experienced, compared to the output of the reference plant.

The effect on plant performance of modelling the atmosphere outside and air inside the chimney of the solar chimney power plant according to different temperature lapse rates was also evaluated. Three different lapse rates, the dry adiabatic lapse rate (DALR), a lapse rate which considers the vapour content of air and a combination of the lapse rate considering vapour content and a lapse rate which takes the effects of condensation into account, are implemented in the numerical model. Results predict (depending on the total collector area covered by vegetation) improved plant performance when considering the effects of air vapour content, compared to the same plant employing a DALR. Further improvement on plant performance is experienced when condensation effects inside the chimney of the plant are taken into account. Despite the improved plant performance when incorporating lapse rates other than the DALR, simulations still predict major reductions in annual plant output of between 30 % and 50 % (compared to the output of the reference plant) as a result of the inclusion of vegetation under the collector roof.

13. Acknowledgements

We would like to thank the National Research Foundation (NRF) and the Volkswagen Stiftung for their financial support.

References

1. *Haaf W, Friedrich K, Mayr G and Schlaich J*, Solar chimneys, part I: Principle and construction of the pilot plant in Manzanares, International Journal of Solar Energy, 1983, 2, 3-20.

2. *Haaf W*, Solar chimneys, part II: Preliminary test results from the Manzanares pilot plant, International Journal of Solar

Energy, 1984, 2, 141-161.
3. *Schlaich J*, The Solar Chimney: Electricity from the Sun, Deutsche Verlags-Anstalt, Stuttgart, 1994.
4. *Pasumarthi N and Sherif SA*, Experimental and theoretical performance of a demonstration solar chimney model – part I: Mathematical model development, *International Journal of Energy Research*, 1998, 22(3), 277-288.
5. *Pasumarthi N and Sherif SA*, Experimental and theoretical performance of a demonstration solar chimney model – part II: Experimental and theoretical results and economic analysis, *International Journal of Energy Research*, 1998, 22(5), 443-461.
6. *Kröger DG and Buys JD*, Performance evaluation of a solar chimney power plant, *ISES 2001 Solar World Congress*, Adelaide, Australia, 2001.
7. *Gannon AJ and Von Backström TW*, Controlling and maximizing solar chimney power output, *1st International Conference on Heat Transfer, Fluid Mechanics and Thermodynamics*, Kruger Park, South Africa, 2002.
8. *Gannon AJ and Von Backström TW*, Solar chimney turbine performance, *Journal of Solar Energy Engineering*, 2003, 125, 101-106.
9. *Bernardes MA dos S, Voß A and Weinrebe G*, Thermal and technical analyses of solar chimneys, *Solar Energy*, 2003, 75(6), 511-524.
10. *Pastohr H, Kornadt O and Gürlebeck K*, Numerical and analytical calculations of the temperature and flow field in the upwind power plant, *International Journal of Energy Research*, 2004, 28, 495-510.
11. *Pretorius JP, Kröger DG, Buys JD and Von Backström TW*, Solar tower power plant performance characteristics, Proceedings of the *ISES EuroSun2004 International Sonnenforum, 1*, Freiburg, Germany, 2004, PSE GmbH, Freiburg, 870-879.
12. *Bilgen E and Rheault J*, Solar chimney power plants for high latitudes, *Solar Energy*, 2005, 79(5), 449-458.
13. *Pretorius JP and Kröger DG*, Solar chimney power plant performance, *Journal of Solar Energy Engineering*, 2006, 128(3), 302-311.
14. *Pretorius JP and Kröger DG*, Sensitivity analysis of the operating and technical specifications of a solar chimney power plant, *Journal of Solar Energy Engineering*, 2007, 129, 171-178.
15. *Kröger DG*, Air-cooled Heat Exchangers and Cooling Towers, Pennwell Corp., Tulsa, Oklahoma, 2004.
16. *Monteith JL and Unsworth MH*, Principles of Environmental Physics, Arnold, London, 1990.
17. *Çengel YA and Boles MA*, Thermodynamics: An Engineering Approach, 3rd Edition, McGraw-Hill, 1998.
18. *Kröger DG and Burger M*, Experimental convection heat transfer coefficient on a horizontal surface exposed to the natural environment, Proceedings of the *ISES EuroSun2004 International Sonnenforum, 1*, Freiburg, Germany, 2004, PSE GmbH, Freiburg, 422-430.
19. *Burger M*, Prediction of the Temperature Distribution in Asphalt Pavement Samples, M.ScEng thesis, University of Stellenbosch, Stellenbosch, South Africa, 2005.
20. *Westdyk D*, evapotranspiration effects on air flowing over grass in a small glass roofed tunnel, MScEng. Thesis, March 2007, University of Stellenbosch, Stellenbosch, South Africa.
21. *Conradie PJ*, Psigrometrie, Unpublished notes, University of Stellenbosch, Stellenbosch, South Africa, 1989.
22. *FAO*, http://www.fao.org/docrep/x0490e/x0490e06.htm, 2006.
23. *Mills AF*, Heat and Mass Transfer, Richard D. Irwin Inc., Chicago, 1995.
24. *Dong A, Grattan SR, Carroll JJ and Prashar CRK*, Estimation of daytime net radiation over well-watered grass, *Journal of Irrigation and Drainage Engineering*, 1992, 118(3), 466-479.
25. *Hsu ST*, Engineering Heat Transfer, D. Van Nostrand Company, Inc., Princeton, New Jersey, 1963.
26. *Taiz L and Zeiger E*, Plant Physiology, 2nd Edition, Sinauer Associates Inc., Sunderland, 1998.
27. *Kröger DG and Blaine D*, Analysis of the driving potential of a solar chimney power plant, *South African Institution of Mechanical Engineering, R & D Journal*, 1999, 15(3), 85-94.

Appendix

A reference solar chimney power plant and typical operating environment is defined by Pretorius and Kröger[13] and its main parameters are repeated here for convenience (see figure 1). The reference site is near Sishen, South Africa, located at latitude 26.67° South and longitude 23.00° East.

Collector roof (Glass)

Emissivity of glass	$e_r = 0.87$
Roughness of glass	$\varepsilon_r = 0$ m
Extinction coefficient of glass	$C_e = 4$ m^{-1}
Refractive index of glass	$n_r = 1.526$
Thickness of glass	$t_r = 0.004$ m
Roof shape exponent	$b = 1$
Perimeter (inlet) height	$H_2 = 5$ m
Outer diameter	$d_2 = 5000$ m
Inner diameter	$d_3 = 400$ m
Inlet loss coefficient	$K_i = 1$
Support diameter	$d_s = 0.2$ m
Support drag coefficient	$C_{sD} = 1$
Support tangential pitch	$P_t = 10$ m
Support radial pitch	$P_r = 10$ m

Ground

Type	Sandstone
Emissivity (treated surface)	$e_g = 0.9$
Absorptivity (treated surface)	$\alpha_g = 0.9$
Density	$\rho_g = 2160$ kg/m^3
Specific heat capacity	$c_g = 710$ J/kgK
Thermal conductivity	$k_g = 1.83$ W/mK
Roughness	$\varepsilon_g = 0.05$ m

Chimney (Concrete)

Height	$H_c = 1000$ m
Inside diameter	$d_c = 210$ m
Bracing wheel (one) drag coefficient	$K_{bw} = 0.01$
Number of bracing wheels	$n_{bw} = 10$
Inside wall roughness	$\varepsilon_c = 0.002$ m

Turbine

Turbo-generator efficiency	$\eta_{tg} = 80$ %
Inlet loss coefficient	$K_{turb,i} = 0.14$

Ambient conditions

Atmospheric pressure	$p_a = 90000$ N/m^2